Pergamon

Int. J. Solids Structures Vol. 33, No. 14, pp. 2095–2118, 1996

0020-7683/96 $15.00 + .00

0020-7683(95)00149-2

SPLINE VARIATIONAL THREE DIMENSIONAL STRESS ANALYSIS OF LAMINATED COMPOSITE PLATES WITH OPEN HOLES

E. V. IARVE*
AdTech Systems Research, Inc., 1342 North Fairfield Road, Beavercreek, OH 45432, U.S.A.

(*Received* 9 *September* 1994; *in revised form* 28 *June* 1995)

Abstract—Independent polynomial spline approximation of displacement and interlaminar tractions is proposed for stress analysis in laminates with open holes. Spline approximation eliminates the inter element compatibility problems leading to unsatisfactory finite element results in the presence of field singularities. Spline approximation offers continuity of displacement, strain and stress fields within homogeneous domains preserving, at the same time, the advantages of local approximation, such as sparsity of the resulting system of equations. Three dimensional full field solution is obtained. Converged stresses and consistent boundary conditions, such as interlaminar traction continuity, are displayed. A closed form asymptotic solution, valid in the vicinity of the hole edge at the interface of two orthotropic plies of arbitrary thickness has been developed to verify the spline approximation based full field solution. Excellent agreement has been observed for interlaminar stresses in a $[45/-45]_s$ AS4/3501-6 laminate under uniaxial tension. The polynomial spline approximation, ideally suited for problems concerned with the singular solution behavior, has been applied to three dimensional stress analysis in practical composites containing tens of plies.

INTRODUCTION

Two dimensional stress analysis of infinite anisotropic plates containing open holes was accomplished by Lekhnitskii (1957). Biaxial loading in combination with loaded hole options was developed by Garbo and Ogonowski (1979) and implemented into a program known as "Bolted Joint Stress Field Model" (BJSFM). This program, based on two dimensional stress calculation and ply level failure analysis using the Tsai–Hill criterion at a characteristic distance from the hole edge, has been used extensively in the aircraft industry for composites. An entire dimension of fundamental composite properties such as stacking sequence, thickness effect, and failure initiation modes (delaminations) have not been considered.

Increased requirements of low weight and high strength in modern aerospace materials require further investigation of the process of failure of composites with holes. To evaluate the possibility of the failure initiation due to delaminations at the free hole edge, analogous to that in classical free edge problem, a three-dimensional stress analysis is required. An assumed stress field near the hole edge was used by Nishioka and Atluri (1982) to design "special-hole-elements" of hybrid finite element formulation. A simple stress distribution function near the hole edge was designed to satisfy the equilibrium equations and boundary conditions. These artificial stresses didn't satisfy the compatibility equations. The results were obtained for $[90/0]_s$ and $[-45/45]_s$ laminates of an idealized composite material.

Raju and Crews (1982) performed a three-dimensional finite element analysis at the hole edge in $[0/90]_s$ and $[90/0]_s$ laminates. The finite element grid was specifically designed to capture interlaminar stress singularities at the hole edge. Displacement approximation by 20-node isoparametric brick elements was used. Calculations were performed with a high density subdivision with 19 000 degrees of freedom in one eighth of the symmetric laminate. The convergence study revealed difficulties in satisfying the transverse normal stress continuity at the ply interface near the hole edge.

*Current address: University of Dayton Research Institute, 300 College Park Avenue, Dayton, OH 45469-0182, U.S.A.

Ericson *et al.* (1984) arrived at a similar conclusion by developing an advanced singular hole element. The singular stress distribution at a given location of the hole edge was assumed to be similar to that at the straight hole edge provided that the ply orientation, with respect to the direction tangential to the hole edge at that location, is same as the ply orientation in the straight edge problem with respect to the edge direction. It is worth mentioning that this assumption has been proven in later studies by Folias (1992) and Wang and Lu (1993). Singular hole element built by combining the singular solution and finite element formulation did not allow the satisfaction of the interlaminar traction continuity at the ply interfaces near the hole edge.

The perturbation technique was used by Bar-Yoseph and Avrashi (1984) to develop the form of the stress field near the hole. Stress finite element analysis was used for interlaminar stress calculation in four ply symmetric laminates. Lucking *et al.* (1984) used a 20-node isoparametric displacement finite element method and sub structuring approach to study the effect of geometry on interlaminar stresses in cross ply composites with circular holes. A sub structuring type approach was used to avoid the tremendous computer resources required for direct stress analysis near the hole edge, even in four ply symmetric composites. Infinite plates were analyzed.

A simplified finite element formulation was given by Chen and Muang (1989). They assumed that the transverse displacement through the thickness of the laminate is constant. However, independent cross-sectional rotations of each layer were allowed. This approach actually didn't take into account the transverse strains and stresses directly. The results were shown to be insensitive to changing the thickness to radius ratio when calculating transverse normal stresses.

Folias (1989) has obtained a local asymptotic solution for three-dimensional stress fields in the immediate vicinity of a bonded interface between isotropic plies and the free edge of a hole. In Folias (1992) these results were extended to orthotropic laminates. The power of interlaminar stress singularity was found to be dependent upon the location at the hole edge. The levels of interlaminar stress singularity determined at the hole edge for a graphite epoxy laminate were found to be an order of magnitude lower than that for isotropic plates determined by Folias (1989). It can possibly be explained by constant transverse normal modulus through the thickness of the laminate. The pioneering work by Wang and Choi (1982) was extended by Wang and Lu (1993) to carry out the asymptotic solution for interlaminar stresses at the hole edge of a composite plate. The stress concentration factors at the hole edge were calculated by using finite element formulation. A $[-45/45]_s$ laminate under uniaxial tension in 0°-direction was treated. The approach was developed under assumption that the ply thickness is much smaller than the hole diameter. We find no full field solution for the addressed problem with converged stresses and consistent boundary conditions, such as interlaminar traction continuity in the literature.

A successful failure onset analysis of composites with open holes is likely to involve a combination of fracture mechanics and failure criteria type parameters. It implies determination of characteristics such as stress intensity factors of the interface singularities along with stress components averaged through certain distances from the hole edge. A full field three-dimensional solution is needed to determine these characteristics under given boundary conditions. Conventional finite element procedures produce field discontinuities at the boundaries of every element. Even the conforming shape functions yield only displacement continuity at the element boundaries. It creates the compatibility problem resulting in stress oscillations of finite element solutions near singularities, as described by Tong and Pian (1973). Sophisticated procedures such as adaptive finite element meshes have been developed recently for solving this problem. The spline approximation offers a simple solution to this problem by eliminating artificial field discontinuities within homogeneous domains. Spline approximation shape functions can be defined to have an arbitrary number of continuous derivatives at nodal points depending upon the order of spline, so that at the nodes inside a homogeneous domain the continuity of displacement as well as strain and stress fields is preserved. At the same time, at the ply interfaces the transverse strain discontinuity is modeled in order to achieve the traction continuity. The advantages of local approximation resulting in a sparse rigidity matrix are maintained by utilizing basic

spline systems with local supporters. This makes the spline approximation approach ideally suited for boundary value problems for multilayered structures with solutions containing regions of singular stress behavior.

The initial development of the through the thickness piece-wise polynomial approximation for two dimensional stress analysis in thick composite beams under dynamic bending was started by Bogdanovich and Iarve (1983). Two and three dimensional formulation of the spline approximation methodology for stress analysis in laminated plates subjected to transverse bending was developed by Bogdanovich and Iarve (1988, 1989a, 1989b, 1990, 1992). Bogdanovich (1991, 1992, 1993) has presented an exhausting overview of modern developments in theory of laminated plates and demonstrated high accuracy and efficiency of spline approximation method (Bogdanovich and Birger, 1992(a,b), 1993, 1994) applied to three-dimensional stress analysis of homogeneous and [0/90/0] composite plates subjected to transverse bending for various boundary conditions.

Independent spline approximation of interlaminar stress components and displacements has been proposed by Iarve and Soni (1993a) for three-dimensional stress analysis of laminates containing open holes. The idea of independent spline approximation of interlaminar stress components was inspired by an assumed stress distribution approach proposed by Pagano (1971, 1978) for straight free edge problems. Analysis of a 24-ply multidirectional laminate with an open circular hole was carried out. The solution was developed in Cartesian coordinates and required unreasonably high numbers of degrees of freedom to provide the desired accuracy of the results at the hole edge. Curvilinear transformation, also based on spline approximation, reported in Iarve and Soni (1993b) and Iarve (1993, 1994), allowed for extension of the spline approximation approach on three dimensional stress prediction in practical composites containing open holes. In the present paper the spline approximation method is extended for stress analysis in regions of singular stress behavior. To verify the accuracy of interlaminar stress prediction near the hole edge an asymptotic solution has been derived. The asymptotic solution is valid in the vicinity of the hole edge at an interface between two orthotropic plies of arbitrary thickness. Good agreement between the asymptotic solution and spline approximation solution for all stress components was observed.

PROBLEM FORMULATION

Consider a rectangular plate consisting of N-orthotropic plies and having a through the thickness opening, shown in Fig. 1. In xyz-coordinates the contour of the opening is defined in parametric form as

$$x = \frac{d}{2}\cos\theta + x_c, \quad y = \frac{d}{2}\sin\theta + y_c, \quad 0 \leqslant \theta \leqslant 2\pi \tag{1}$$

where d is the hole diameter and x_c, y_c the hole center coordinates. θ is the polar angle measured from the x-direction. The center of the polar coordinate r, θ, z system coincides

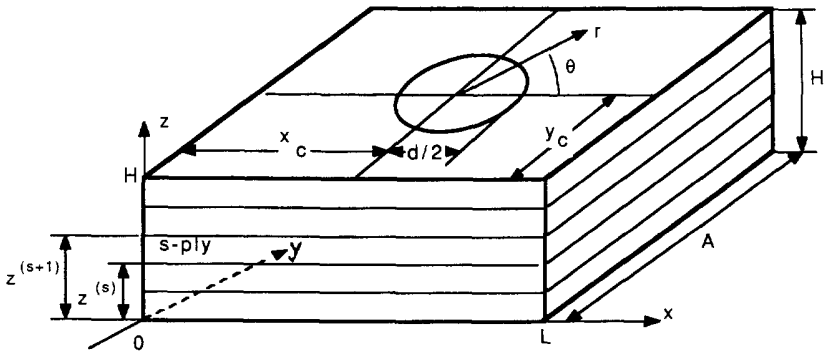

Fig. 1. Laminated plate with a hole. Coordinate systems and dimensions.

with the center of the hole. The plate is of length L in the x-direction and width A in the y-direction. Displacement boundary conditions are applied at lateral edges $x = 0, L$ as follows

$$u_x(0, y, z) = -u_x(L, y, z) = -\Delta,$$
$$u_y(0, y, z) = -u_y(L, y, z) = u_z(0, y, z) = -u_z(L, y, z) = 0. \tag{2}$$

$\Delta > 0$ introduces tensile loading in the x-direction. Zero values of the u_y and u_z displacements are used as realistic simulations of the experimental conditions at the grips. The interlaminar surfaces between s and $s+1$ plies are denoted as $z = z^{(s)}$, where $z^{(0)} = 0$, $z^{(N)} = H$, where H = thickness of the plate. Surfaces $z = z^{(0)}$ and $z = z^{(N)}$ are traction free, along with the lateral edges $y = 0$, $y = A$ and the hole edge.

A full field three dimensional solution will be obtained based on spline approximation of displacement and interlaminar stress components in curvilinear coordinates. It will be shown that the stress distributions recovered near the hole edge and interface between plies match the close form asymptotic solution results.

Utilization of spline functions of n-th degree allows the provision of an $n-1$ times continuously differentiable displacement approximation through the entire ply. For $n \geqslant 3$ the strain and stress components will be continuous through the homogeneous ply. The weak form solution (minimum of the potential energy) over a class of twice continuously differentiable displacement functions and the strong form solution (point-wise solution of the equilibrium equations) are known to coincide, provided that both exactly satisfy the boundary conditions. For each ply of the plate the displacement boundary conditions are specified at the surface $x = 0, L$. These conditions will be satisfied exactly for all approximation functions. The traction boundary conditions are specified at the open hole edge, on edges $y = 0, A$ and surfaces $z = z^{(s-1)}$, $z = z^{(s)}$, where s is the ply number. Non zero tractions, applied at the surfaces $z = z^{(s-1)}$, $z = z^{(s)}$, are independently approximated also by using spline functions and assumed to be fixed parameters when the ply equations are derived. They are calculated by applying boundary conditions of displacement and traction continuity at the ply surfaces. For every ply, the solution accuracy can be monitored by the accuracy of point wise satisfying the zero traction boundary conditions at the hole edge and $y = 0, A$ and the non-zero boundary conditions at the ply surfaces.

In each ply, displacement components u_x, u_y and u_z are approximated as functions of generalized coordinates ρ, ϕ and z ($0 \leqslant \rho \leqslant 1$, $0 \leqslant \phi \leqslant 2\pi$, $0 \leqslant z \leqslant H$), where $x = x(\rho,\phi)$, $y = y(\rho,\phi)$ and $z = z$. A procedure to build a set of basic spline functions appropriate for boundary value applications will be considered below. Generally the linear approximation of displacement components in the s-th ply can be expressed as

$$u_x^{(s)}(\rho, \phi, z) = \boldsymbol{\chi}_1^{(s)}(\rho, \phi, z)\mathbf{U}_s^*, \quad u_y^{(s)}(\rho, \phi, z) = \boldsymbol{\chi}_2^{(s)}(\rho, \phi, z)\mathbf{V}_s^*, \quad u_z^{(s)}(\rho, \phi, z) = \boldsymbol{\chi}_3^{(s)}(\rho, \phi, z)\mathbf{W}_s^* \tag{3}$$

The superscript star means transpose of a matrix or a vector. Components of the vectors $\boldsymbol{\chi}_i^{(s)}(\rho, \phi, z)$ are three-dimensional spline functions. The vectors $\mathbf{U}_s$, $\mathbf{V}_s$, $\mathbf{W}_s$ contain unknown spline approximation coefficients. Different spline functions can be used for different displacement components depending upon the boundary conditions. The approximation (3) is assumed to provide kinematically admissible displacements, i.e. satisfying the boundary conditions (2), for any combination of spline approximation coefficients $\mathbf{U}_s$, $\mathbf{V}_s$, $\mathbf{W}_s$. The interface tractions at the bottom: $z = z^{(s-1)}$, and top: $z = z^{(s)}$, surfaces of the s-th ply are denoted as $p_i^{(s_1)}$, $s_1 = s-1, s$:

$$p_i^{(s_1)}(\rho, \phi) = (-1)^{(s-s_1)}\sigma_{z\mu_i}(\rho, \phi, z^{(s_1)}), \quad i = 1, 2, 3; \quad \mu_1 = x, \quad \mu_2 = y, \quad \mu_3 = z,$$

where $s = 1, \ldots, n$ is the ply number. Their spline approximation is introduced similar to the displacement approximation:

$$p_i^{(s_1)}(\rho,\phi) = \chi_i^{(s)}(\rho,\phi,z^{(s_1)})\mathbf{T}_i^{(s_1)*}; \quad i=1,2,3; \quad s_1 = s-1, s; \quad s=1,\ldots,N. \tag{4}$$

The utilization of the same spline approximation basic functions for related displacement and traction components avoids the over definition of the problem by defining surface tractions and displacements at the same locations. The potential energy of the s-th ply can be written as

$$\Pi^{(s)} = \int_0^1 \mathrm{d}\rho \int_0^{2\pi} \left(\int_{z^{(s-1)}}^{z^{(s)}} \tfrac{1}{2}\sigma_{ij}\varepsilon_{ij}\,\mathrm{d}z - \sum_{s_1=s-1}^{s} p_i^{(s_1)} u_{\mu_i}^{(s)}(\rho,\phi,z^{(s_1)}) \right) \det \mathbf{J}\,\mathrm{d}\phi + \int_{S_t} T_{\mu_i} u_{\mu_i}^{(s)}\,\mathrm{d}A \tag{5}$$

where summation is implied upon the indexes $i,j = 1, 2, 3$. $\mathbf{J}$ is the Jacobean matrix of the curvilinear transformation. σ_{ij} and ε_{ij} are the stress and strain components of the s-th ply in xyz-coordinates (directions 1, 2, 3 correspond to x, y, z respectively) expressed through the displacement spline approximation coefficients and stiffness coefficients. The strain components are calculated by direct differentiation of expressions (3) point-wise:

$$\begin{aligned}
&\varepsilon_{11} = [D_x\chi_1^{(s)}(\rho,\phi,z)]\mathbf{U}_s^*, \quad \varepsilon_{13} = \left[\frac{\partial}{\partial z}\chi_1^{(s)}(\rho,\phi,z)\right]\mathbf{U}_s^* + [D_x\chi_3^{(s)}(\rho,\phi,z)]\mathbf{W}_s^*,\\
&\varepsilon_{22} = [D_y\chi_2^{(s)}(\rho,\phi,z)]\mathbf{V}_s^*, \quad \varepsilon_{23} = \left[\frac{\partial}{\partial z}\chi_2^{(s)}(\rho,\phi,z)\right]\mathbf{V}_s^* + [D_y\chi_3^{(s)}(\rho,\phi,z)]\mathbf{W}_s^*,\\
&\varepsilon_{33} = \left[\frac{\partial}{\partial z}\chi_3^{(s)}(\rho,\phi,z)\right]\mathbf{W}_s^*, \quad \varepsilon_{12} = [D_x\chi_2^{(s)}(\rho,\phi,z)]\mathbf{V}_s^* + [D_y\chi_1^{(s)}(\rho,\phi,z)]\mathbf{U}_s^*.
\end{aligned} \tag{6}$$

Differential operators D_x and D_y provide differentiation in the x and y direction in curvilinear coordinates. The stress components in every point are related to strains by Hooke's law:

$$\sigma_{ij} = Q_{ijkl}^{(s)}(\varepsilon_{kl} - t_{kl}^{(s)}\Delta T) \tag{7}$$

where ΔT is uniform temperature change and $t_{kl}^{(s)}$ are thermal expansion coefficients. The second integral in the right hand side of eqn (5) taken over area S_t accounts for the work of external tractions which can be applied at the hole edge and the ply edges.

A system of equations allowing for the calculation of the displacement spline approximation coefficients under given surface tractions is obtained by using the minimum potential energy principle. Then the displacement and traction continuity conditions at the interfaces are imposed and the single ply equations combined into the global system of equations. The displacement spline approximation coefficients in all plies can be calculated by solving this system of equations. This system will not contain the interlaminar tractions, because they cancel out by summation of the ply equations. After displacement spline approximation coefficients are obtained, the traction spline approximation coefficients can be obtained from single ply equations.

The present solution provides all displacement, strain and stress components in every point of the laminate. The displacement values at every point can be obtained using eqn (3). Inside each ply, continuous strain and stress values at each point are given by eqns (6) and (7). Thus, at the ply interface two values of each stress component can be calculated, one in the lower and one in the upper ply. For the exact displacement field the transverse interlaminar stress component in each ply has to be equal to the traction value obtained by using eqn (4) at the same location. The discrepancy between these values is a measure of the approximation error. A detailed investigation of stress fields is performed below.

CURVILINEAR TRANSFORMATION

Generalized curvilinear coordinates ρ and ϕ are introduced to map the x, y cross-section of the plate with an opening onto a rectangular region $0 \leqslant \rho \leqslant 1$, $0 \leqslant \phi \leqslant 2\pi$. For $\rho = 0$, this transformation will describe the contour of the opening, given by eqn (1). For $\rho = 1$, it will describe the rectangular contour of the plate. The transformation is defined as:

$$x = \frac{d}{2}F_1(\rho)\cos\phi + L \cdot F_2(\rho)\alpha(\phi) + x_c, \quad 0 \leqslant \rho \leqslant 1, \tag{8}$$

$$y = \frac{d}{2}F_1(\rho)\sin\phi + A \cdot F_2(\rho)\beta(\phi) + y_c, \quad 0 \leqslant \phi \leqslant 2\pi.$$

Functions $\alpha(\phi)$ and $\beta(\phi)$ are defined so that the parametric equations:

$$x = L \cdot \alpha(\phi) + x_c, \quad y = A \cdot \beta(\phi) + y_c, \quad 0 \leqslant \phi \leqslant 2\pi \tag{9}$$

describe the rectangular boundary of the plate. Functions $F_1(\rho)$ and $F_2(\rho)$ provide a smooth transition between contours (1) and (9) for the ρ-values changing from 0 to 1. They are defined so that in the vicinity of the hole $d/2 \leqslant r \leqslant (1+\kappa)d/2$, where typically $\kappa = 2$, transformation (8) will become similar to polar coordinate transformation, i.e. $\phi = \theta$ and the distance from the center of the hole is a linear function of ρ. Functions $F_1(\rho)$ and $F_2(\rho)$ are defined as follows:

$$F_1(\rho) = \left\{ \begin{array}{c} 1 + \dfrac{\kappa}{\rho_h}\rho, \rho \leqslant \rho_h, \\ \dfrac{(1+\kappa)(1-\rho)}{1-\rho_h}, \rho_h < \rho \leqslant 1 \end{array} \right\}, \quad F_2(\rho) = \left\{ \begin{array}{c} 0, \rho \leqslant \rho_h, \\ \dfrac{\rho - \rho_h}{1-\rho_h}, \rho_h < \rho \leqslant 1 \end{array} \right\}.$$

The near hole region $d/2 \leqslant r \leqslant (1+\kappa)d/2$ apparently corresponds to $0 \leqslant \rho \leqslant \rho_h$, where $\rho_h (0 \leqslant \rho_h \leqslant 1)$ is arbitrary and defines the part of the interval between 0 and 1 which transforms into the near hole region. The functions F_1 and F_2 will be approximated by using polynomial splines. Linear functions can be approximated by splines of degree $n \geqslant 1$ exactly. In the region of slope change, i.e., near $\rho = \rho_h$, spline approximation will smooth the slope discontinuities providing the continuity of the Jacobean matrix of the transformation (8) through the entire plate. Functions $\alpha(\phi)$, $\beta(\phi)$ are defined as follows:

$$\alpha(\phi - \phi_h) = \left\{ \begin{array}{ll} \left(1 - \dfrac{x_c}{L}\right)\dfrac{\phi^{(1)} - \phi}{\phi^{(1)}}, 0 \leqslant \phi \leqslant \phi^{(1)}; & \left(1 - \dfrac{x_c}{L}\right)\dfrac{\phi - \phi^{(2)}}{\phi^{(3)} - \phi^{(2)}}, \phi^{(2)} < \phi \leqslant \phi^{(3)}; \\ 0, \phi^{(1)} < \phi \leqslant \phi^{(2)}; & \left(1 - \dfrac{x_c}{L}\right), \phi^{(3)} < \phi \leqslant 2\pi; \end{array} \right\},$$

$$\beta(\phi - \phi_h) = \left\{ \begin{array}{ll} \left(1 - \dfrac{y_c}{A}\right), 0 \leqslant \phi \leqslant \phi^{(1)}; & 0, \phi^{(2)} < \phi \leqslant \phi^{(3)}; \\ \left(1 - \dfrac{y_c}{A}\right)\dfrac{\phi^{(2)} - \phi}{\phi^{(2)} - \phi^{(1)}}, \phi^{(1)} < \phi \leqslant \phi^{(2)}; & \left(1 - \dfrac{y_c}{A}\right)\dfrac{\phi - \phi_3^{(3)}}{2\pi - \phi^{(3)}}, \phi^{(3)} < \phi \leqslant 2\pi; \end{array} \right\},$$

$$\phi_h = \arctan\frac{A - y_c}{L - x_c}.$$

The length of the intervals between 0, $\phi^{(1)}$, $\phi^{(2)}$, $\phi^{(3)}$, 2π is determined proportional to the A/L ratio. These functions are also approximated by using cubic splines. The distortion of the shape of the rectangular plate due to spline approximation of $\alpha(\phi)$ and $\beta(\phi)$ is negligible and will be shown in numerical examples.

CONSTRUCTION OF THE BASIC SPLINE FUNCTIONS FOR SOLVING THE BOUNDARY VALUE PROBLEMS

Polynomial spline approximation is the most general type of polynomial approximation. Polynomial spline of degree n over an interval $[a,b]$ with subdivision $a = x_0 < x_2 < x_3 \ldots < x_m = b$ is an arbitrary piece-wise polynomial of degree less than or equal to n at the intervals $x_{i-1} \leqslant x \leqslant x_i$, $i = 1, \ldots, m$. If a spline is constructed so that at every internal node x_i, $i = 1, \ldots m-1$ it has $n-\delta_i$ continuous derivatives, than δ_i is called the defect of spline in the node x_i. The lower the defect, the smoother is the spline function. The totality of all polynomial splines of degree n over an interval $[a,b]$ with subdivision $a = x_0 < x_2 < x_3 \ldots < x_m = b$ with defects $\delta_i < \delta$ forms a linear space of dimension $m\delta + n - \delta + 1$. A given spline function will be equal to zero at most of the subintervals $x_i \leqslant x \leqslant x_{i-1}$. Those subintervals at which a spline is different from zero are called its local supporter. The degree of spline, the subdivision and the defect are defined by the application needs. For practical solutions of boundary value problems a set of basic spline functions has to be constructed in order to represent the displacement and interlaminar stress components as their linear combination and obtain the unknown coefficients by using variational principles. To provide the sparsity of the resulting system of equations, these basic functions have to have local supporters of minimum length. A recurrent procedure has been initially proposed by Bogdanovich and Iarve (1988) to construct a set of quadratic spline functions suited for applications in boundary value problems. Straight forward generalization of the procedure for splines of arbitrary degree has been developed by the same authors in later papers (1990, 1992). Fundamental properties of the n-th degree splines near the interval boundaries are described below. The procedure is based on subsequent integration of lower order basic splines followed by superposition to maintain the local supporters and boundary properties. A set of zero order $n = 0$ spline functions is defined as

$$X_{0,i}(x) = 1, \quad x_i \leqslant x \leqslant x_{i-1} \quad \text{and} \quad X_{0,i}(x) = 0, \quad x_{i-1} > x, \quad x > x_i, \quad i = 1, \ldots, m.$$

Defect $\delta = 1$ in this particular case means that even the zero order derivative, i.e. the value of the spline function, can be discontinuous at the nodes. Splines $X_{0,i}(x)$ apparently satisfy the following properties for $n = 0$. All $X_{n,i}(x)$ are completely defined inside the interval $[a,b]$ and

$$\begin{gathered} X_{n,1}(x_0) = X_{n,n+m}(x_m) = 1, \\ X_{n,n+m}(x_0) = X_{n,1}(x_m) = X_{n,j}(x_0) = X_{n,j}(x_m) = 0, \quad j = 2, n+m-1; \\ \sum_{j=1}^{n+m} X_{n,j}(x) = 1, \quad a \leqslant x \leqslant b. \end{gathered} \tag{10}$$

The following recurrent procedure allows the building of a system of basic spline functions of arbitrary degree n and defect $\delta = 1$ maintaining the above formulated properties:

$$X_{n+1,i}(x) = \frac{I_{n,i-1}(x)}{I_{n,i-1}(x_m)} - \frac{I_{n,i}(x)}{I_{n,i}(x_m)}, \quad i = 2, \ldots, n+m;$$

$$X_{n+1,1}(x) = 1 - \frac{I_{n,1}(x)}{I_{n,1}(x_m)}, \quad X_{n+1,n+1+m}(x) = \frac{I_{n,n+m}(x)}{I_{n,n+m}(x_m)},$$

where

$$I_{n,i}(x) = \int_a^x X_{n,i}(\tau)\,\mathrm{d}\tau.$$

All spline functions calculated using this procedure are completely defined inside the interval $[a, b]$ and have a local supporter maximum of $n+1$ intervals. Splines $X_{n,i}$, $n < i < m$ are equal to B-splines within arbitrary multiplicative factors. Splines $X_{n,i}$ and $X_{n,n+m+1-i}$, $i \leqslant n$ have a local support of i-intervals. The boundary conditions at the ends of their local supporters are:

$$\frac{\mathrm{d}^v}{\mathrm{d}x^v} X_{n,n+m+1-i}(x_m) = \frac{\mathrm{d}^v}{\mathrm{d}x^v} X_{n,i}(x_0) = 0, \quad v \leqslant i-2; \tag{11}$$

$$\frac{\mathrm{d}^v}{\mathrm{d}x^v} X_{n,n+m+1-i}(x_{m-i}) = \frac{\mathrm{d}^v}{\mathrm{d}x^v} X_{n,i}(x_i) = 0, \quad v \leqslant n-1.$$

These splines possess a fundamental property similar to B-splines, they have a supporter of minimum length under boundary conditions (11). The properties (10), (11) at the ends of the interval are practically important for boundary value problem applications and allow to impose boundary conditions at the ends of the interval $x = a$ and $x = b$ in a straight forward way. For example, an unknown function $F(x)$ satisfies simple Derichlet type boundary conditions $F(a) = F(b) = 0$. Then, according to boundary property (10), a truncated system of spline functions has to be used for approximation, so that

$$F(x) = \sum_{i=2}^{n+m-1} f_i X_{n,i}(x).$$

This truncated system can not contain spline functions: $X_{n,1}$ and $X_{n,n+m}$. The boundary conditions $F(a) = F(b) = 0$ are satisfied for any combination of coefficients f_i, whereas, by using a set of basic spline functions containing only B-splines these boundary conditions have to be applied by using Lagrangian multipliers, leading to excessive number of degrees of freedom and cumbersome formulations for three dimensional problems.

In applications dealing with discontinuous material properties, splines with defect $\delta_p = \delta$, $1 < \delta \leqslant n$ in specified internal node x_p, $0 < p < m$, and with defect $\delta_i = 1$, $i \neq p$ in all other internal nodes might be required. A two step procedure to build such splines is utilized. At the first step we consider two independent intervals: $[a, x_p]$ and $[x_p, b]$. On each of these intervals we build a system of spline functions of degree equal to δ and defect $\delta_i = 1$ ($1 \leqslant i \leqslant p-1$, $p+1 \leqslant i \leqslant m-1$) by applying the recurrent procedure. After that we combine the two sets of spline functions into one set by numbering first the $p+\delta$ splines of the interval $[a, x_p]$ and then $(m-p)+\delta$ splines of the interval $[x_p, b]$. Second step consists of applying the recurrent procedure $n-\delta$ times at the entire interval $[a, b]$ to the set of $m+2\delta$ functions obtained at the first step. As a result, we obtain a set of $m+n+\delta$ spline functions of n-th degree. Note that the two step procedure for $\delta = 1$ doesn't coincide with the original one step procedure over the entire interval. The spline functions in the vicinity of the node x_p differ from regular B-splines. They possess a fundamental property similar to B-splines and splines (11), namely they have a local supporter of minimum length under the boundary conditions similar to those for the B-splines, but having a defect $\delta_p = \delta > 1$ at one of the internal nodes. In case if higher defect is required at more than one internal node of the interval $[a, b]$, the first step has to be performed independently on each subinterval between the nodes with higher defect.

Cubic spline approximation with defect equal to 1 has been utilized for displacement approximation. Cubic splines $X_{3,i}$ with defect $k = 1$ built over an interval $0 \leqslant x \leqslant 1$ subdivided uniformly into 7 intervals are shown in Fig. 2.

Subdivisions through the thickness of each ply and ρ-coordinate are introduced as follows:

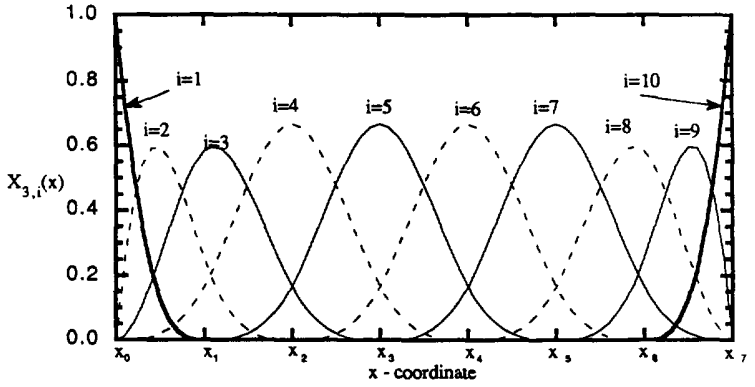

Fig. 2. System of basic cubic splines with nodes $x_0 < x_1 < \cdots < x_7$ built for boundary value problem applications.

$$z^{(s-1)} = z_0 < z_1 < z_2 < \cdots < z_{n_s} = z^{(s)}, \quad 0 = \rho_0 < \rho_1 < \rho_2 < \rho_3 \cdots < \rho_m = 1. \quad (12)$$

Cubic splines $\{Z^{(s)}i(z)\}$, $i = 1, \ldots, n_s+3$, built according to the recurrent procedure were used in the z-direction through the thickness of the s-th ply, $s = 1, \ldots, N$ (n_s is the number of sublayers in the s-th ply). A set of cubic splines $\{R_i(\rho)\}$, $i = 1, \ldots, m+3$ (m is the number of intervals in the ρ-direction) has been built to approximate the dependence of the displacement components upon the ρ-coordinate.

The spline approximation in ϕ-direction represents a special case. Periodicity boundary conditions have to be satisfied at the ends of the interval:

$$\frac{d^v}{d\phi^v}F(0) = \frac{d^v}{d\phi^v}F(2\pi) = 0, \quad v = 0, 1 \ldots.$$

A standard approach has been taken. The interval has been subdivided into k-subintervals and extended beyond its ends, so that:

$$0 = \phi_0 < \phi_1 < \phi_2 < \phi_3 \ldots < \phi_k = 2\pi; \quad \phi_{-i} = \phi_{k-i} - 2\pi, \quad \phi_{k+i} = \phi_i + 2\pi, \quad i = 1, 2, 3.$$

A set of $(k+6)+3$ basic cubic spline functions $\{\bar{\Phi}_i\}$, $i = -2, \ldots, k+6$ is built on the extended interval $\phi_{-3} \leqslant \phi \leqslant \phi_{k+3}$ by using the recurrent procedure. Spline approximation of an arbitrary function within the initial interval $0 \leqslant \phi \leqslant 2\pi$ can be written as

$$F(\phi) = \sum_{i=1}^{k+3} f_i \bar{\Phi}_i(\phi).$$

To provide the periodicity boundary conditions for an arbitrary function the following is required: $f_i = f_{k+i}$, $i = 1, 2, 3$. Thus the above approximation is modified as

$$F(\phi) = \sum_{i=1}^{k} f_i \Phi_i(\phi), \; \Phi_i(\phi) = \bar{\Phi}_i(\phi) + \bar{\Phi}_{k+i}(\phi), \; i = 1, 2, 3; \quad \Phi_i(\phi) = \bar{\Phi}_i(\phi), \; i = 4, \ldots, k.$$

This approximation satisfies the periodicity boundary conditions for arbitrary set of coefficients f_i. The modified set of spline functions $\{\Phi_i(\phi)\}$, $i = 1, \ldots, k$ is used for displacement approximation in ϕ-direction. Splines in ρ and ϕ-directions are used for approximation of the interlaminar stress components at the interfaces as well.

SPLINE APPROXIMATION OF DISPLACEMENT AND INTERLAMINAR STRESS COMPONENTS

Vectors of spline functions for three dimensional spline approximation along ρ, ϕ and z coordinates in the s-th ply can be expressed as:

$$\{\chi^{(s)}\}_M = R_l(\rho)\Phi_j(\phi)Z_l^{(s)}(z), \quad M = l+(j-1)(n_s+3)+(i-1)(n_s+3)k;$$
$$l = 1,\ldots,n_s+3; \quad j = 1,\ldots,k; \quad i = 1,\ldots,m+3.$$

To satisfy the boundary conditions (2), certain displacement approximation coefficients have to be assigned constant values. The modified approximation can be expressed generally by introducing non square boundary matrices $\mathbf{C}_1^{(s)}, \mathbf{C}_2^{(s)}, \mathbf{C}_3^{(s)}$:

$$u_x^{(s)}(\rho,\phi,z) = \mathbf{C}_1^{(s)}\chi^{(s)}(\rho,\phi,z)\mathbf{U}_s^* + \chi^{(s)}(\rho,\phi,z)\mathbf{E}^*\Delta, \tag{13}$$
$$u_y^{(s)}(\rho,\phi,z) = \mathbf{C}_2^{(s)}\chi^{(s)}(\rho,\phi,z)\mathbf{V}_s^*, \quad u_z^{(s)}(\rho,\phi,z) = \mathbf{C}_3^{(s)}\chi^{(s)}(\rho,\phi,z)\mathbf{W}_s^*.$$

Vector $\mathbf{E}$ is defined so that $\{\mathbf{E}\}_M = 1$ if $\{\chi(1,\phi,z)\}_M \neq 0$ for $\phi^{(1)} < \phi < \phi^{(2)}$ and $\{\mathbf{E}\}_M = -1$ if $\{\chi(1,\phi,z)\}_M \neq 0$ for $\phi^{(3)} < \phi < 2\pi$. All other components are equal to zero. Accounting for the properties of the spline functions (10) we observe that the approximation (13) satisfies the boundary conditions (2) if $\mathbf{U}_s = 0$. The non square boundary matrices $\mathbf{C}_1^{(s)}$ are introduced to define the truncated system of spline functions so that the displacement components given in (13) satisfy the boundary conditions (2) for an arbitrary set of spline approximation coefficients. Analogously to Derichlet type of boundary conditions, considered in previous section, the components of spline approximation vector contributing at the sides $x = 0$ and $x = L$ need to be excluded. $\mathbf{C}_1^{(s)}$ is constructed in the following way. It is initially assumed to be a unit matrix then the number of rows is reduced by skipping all rows having nonzero scalar product with $\mathbf{E}^*$. Thus, for any vector of spline approximation coefficients $\mathbf{U}_s$ the approximation satisfies conditions (2). According to boundary conditions (2): $\mathbf{C}_1^{(s)} = \mathbf{C}_2^{(s)} = \mathbf{C}_3^{(s)}$. Spline approximation of the interlaminar tractions can be expressed as:

$$p_i^{(s_1)}(\rho,\phi) = \mathbf{C}_i^{(s)}\chi^{(s)}(\rho,\phi,z^{(s_1)})\mathbf{T}_i^{(s_1)*}, \quad i = 1,2,3; \quad s_1 = s-1,s; \quad s = 1,\ldots,N. \tag{14}$$

The system of equations for determination of the unknown coefficients of displacement spline approximation is obtained by applying the minimum potential energy principle provided that surface tractions are given:

$$\mathbf{B}_{i1}^{(s)}\mathbf{U}_s + \mathbf{B}_{i2}^{(s)}\mathbf{V}_s + \mathbf{B}_{i3}^{(s)}\mathbf{W}_s = \mathbf{Q}_i^{(s)}\Delta + \sum_{s_1=s-1}^{s} \mathbf{C}_i^{(s)}\mathbf{D}^{(s)}\mathbf{C}_i^{(s)*}\mathbf{T}_i^{(s_1)}, \quad i = 1,2,3. \tag{15}$$

The components of the matrices $\mathbf{B}_{ij}^{(s)}$ depend upon the stiffness properties and geometry and the components of the loading vector $\mathbf{Q}_i^{(s)}$ depend upon the geometric parameters. The components of the square matrices $\mathbf{D}^{(s)}$ are defined as

$$\mathbf{D}^{(s_1)} = \int_0^1 \mathrm{d}\rho \int_0^{2\pi} \chi^{(s)}(\rho,\phi,z^{(s_1)}) \otimes \chi^{(s)}(\rho,\phi,z^{(s_1)}) \det \mathbf{J}\, \mathrm{d}\phi, \quad s_1 = s-1,s.$$

Symbol $\otimes$ means a tensor product of the vectors. The displacement spline approximation coefficients are calculated from the global system of equations obtained by combining systems (15) for all plies and imposing the continuity of tractions and displacements at the interfaces. Due to traction continuity all traction terms in the right side cancel out and the global system will contain only displacement approximation coefficients. After they are obtained, the traction spline approximation coefficients can be obtained by resolving

the ply eqns (15) against $\mathbf{T}_i^{(s_1)}$ starting from the outer ply $s = 1$ and knowing that $\mathbf{T}_1^{(0)} = \mathbf{T}_2^{(0)} = \mathbf{T}_3^{(0)} = 0$, according to boundary conditions at the surfaces $z = 0$ and $z = H$.

Exactly the same system of equations for calculating the displacement spline approximation coefficients obtained after combining ply equations and imposing interlaminar continuity conditions can also be obtained by approximating the displacement components in the z-direction with splines built using the two step recurrent procedure, described in the previous section. In this case the spline functions in the z-direction are built on the interval $[0, H]$. At the first step this interval is separated into N (number of plies) subintervals: $[z^{(s-1)}, z^{(s)}]$, $s = 1, \ldots, N$, with nodes (12). By applying the two step procedure a system of cubic splines with defects $\delta_{I_s} = 2, \mathrm{I}_s = \Sigma_{i=1}^{s} n_i, s = 1, \ldots, N-1$ and $\delta = 1$ in all other nodes is obtained to describe the laminate.

Potential energy expression (5) will be valid if $z^{(s-1)} = 0$ and $z^{(s)} = H$. It will be shown below that the interlaminar tractions calculated through the ply eqns (15), provided by independent displacement and interlaminar traction spline approximation approach, are detrimental for accurate interlaminar stress calculation near field singularities.

STRESS CALCULATION AND COMPARATIVE STUDY

Strains and stresses at every point of the plate are directly calculated by using formulas (6) and (7) after the displacement spline approximation coefficients were obtained through the variational procedure given above. The cubic splines used for displacement approximation in every ply are continuously differentiable two times at all points inside the ply. Thus, all strain components will be continuous inside each ply. The same holds for stress components directly obtained by using Hooke's law at all points. The transverse strains calculated in adjacent plies at their common interface may be discontinuous. The corresponding stress components may also be discontinuous. However, the transverse stress components must be equal to the same traction value obtained from (14) to satisfy the equilibrium at the interface. This condition and the zero traction conditions at the hole edge appear in present approach as a natural boundary condition. The accuracy to which it is satisfied is mesh dependent. To study the convergence in the vicinity of the hole edge a symmetric AS4/3501-6 laminate $[45/-45]_s$ was considered. The plate was $L = 63.5$ mm long, $A = 31.75$ mm wide, $H = 1.16$ mm thick and contained a 6.35 mm diameter central hole. The plies had the following elastic properties: $E_1 = 139$ GPa, $E_2 = E_3 = 10.34$ GPa, $G_{12} = G_{31} = 5.52$ GPa, $G_{23} = 3.31$ GPa, $\nu_{12} = \nu_{13} = 0.3$, $\nu_{23} = 0.55$. The upper half of the laminate was modeled. Upon ϕ-coordinate, a uniform subdivision in $k = 24$ intervals was used.

Different out of plane subdivisions were considered. Subdivisions #1 had one interval per play: $n_1 = n_2 = 1$. Subdivision #2 contained three intervals through the thickness of each ply, so that in the first ply: $(z_1 - z_0) : (z_2 - z_1) : (z_3 - z_2) = 1 : 2 : 1$. The second ply was subdivided similarly. Subdivision #3 had six intervals per ply, so that in the first ply $(z_1 - z_0) : (z_2 - z_1) : (z_3 - z_2) : (z_4 - z_3) : (z_5 - z_4) : (z_6 - z_5) = 1 : 1 : 2 : 2 : 1 : 1$. The second ply was subdivided similarly.

Non-uniform subdivision was also used in the ρ-direction. The diameter of the near hole region, where the transformation (8) is quasi polar, was always equal to $3d(\kappa = 2)$. The number of intervals of subdivision inside this region is denoted m_0: $\rho_h = \rho_{m_0}$. The interval $0 \leqslant \rho \leqslant 1$ was subdivided so that:

$$q = \frac{\rho_{i+1} - \rho_i}{\rho_i - \rho_{i-1}}, \quad i = 1, \ldots, m-1.$$

Mesh #1 had total of $m = 10$ intervals and $m_0 = 6$. The number of intervals in the near hole region was $m_0 = 6$ and the interval size ratio: $q = 1.2$. Mesh #2 was formed similarly by using $m = 14$, $m_0 = 10$ and $q = 1.2$. The higher density mesh #3 was formed by $m = 24$ intervals, $m_0 = 20$ and $q = 1.5$. The sizes of the shortest interval $(\rho_1 - \rho_0)$ near

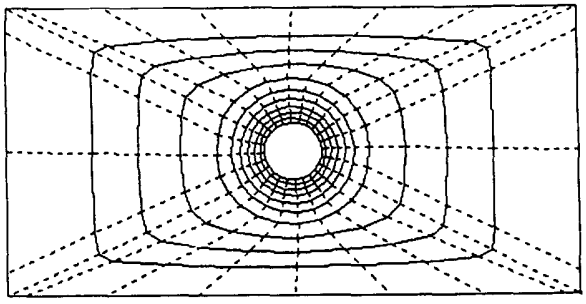

Fig. 3. Coordinate lines of the curvilinear approximation (3): ρ = const. (solid lines), ϕ = const. (dashed lines).

the hole edge were $0.1927 \times 10^{-1} d$; $0.8446 \times 10^{-2} d$; $0.14851 \times 10^{-4} d$ for meshes #1, 2 and 3 respectively.

The coordinate lines of curvilinear transformation for mesh #1 are shown in Fig. 3. The transformation functions $F_1(r)$, $F_2(r)$, $\alpha(\phi)$, $\beta(\phi)$ are approximated by using the spline functions. The distortion of the rectangular boundary due to this approximation is negligible. The displacement boundary condition (2) was applied and $\Delta = 10^{-5}$ mm. The average uniaxial stress in the loading direction was calculated as

$$\sigma_0 = \frac{1}{H \cdot A}\left|\int_0^H \mathrm{d}z \int_{\phi^{(1)}}^{\phi^{(2)}} \sigma_{xx}(0, \phi, z) \frac{\partial y}{\partial \phi} \mathrm{d}\phi\right|.$$

This value was used to normalize the stress components shown below.

The stress components at the hole edge in the middle of the ply were considered first. The circumferential stresses $\sigma_{\theta\theta}$ at the hole edge in the middle of the -45° and the 45° plies are shown in Fig. 4. These calculations were performed using subdivision #2 through the thickness. The results obtained for meshes number 2 and 3 are practically identical. The radial and in-plane shear stresses in the middle of the -45° ply, also shown in this figure, illustrate the accuracy of satisfying the natural boundary conditions even by using the coarsest mesh. Figure 5 shows the transverse shear stresses $\sigma_{\theta z}$ and σ_{rz} at the hole edge in the middle of the 45° ply. The subdivision #2 was used through the thickness. The accuracy of satisfying the boundary condition $\sigma_{rz} = 0$ is sensitive to the mesh refinement even though the values of $\sigma_{\theta z}$ stress obtained with the meshes 1, 2 and 3 are practically same. The results shown above were recalculated with subdivision #1 and found to be insensitive to changing the out of plane subdivision. A significant effect of the number of sublayers through the thickness was observed on the values of transverse normal stress σ_{zz}. The values of σ_{zz} calculated at the hole edge on the mid-surface of the laminate by using the mesh #1 and three different subdivisions through the thickness are shown in Fig. 6a. Similar studies were performed for meshes number 2 and 3. It was established that the results observed for

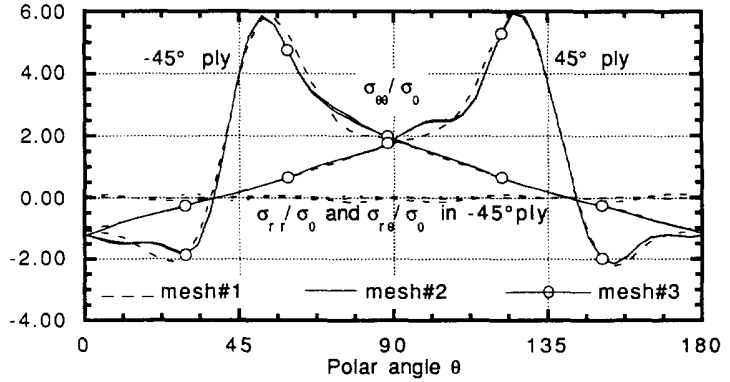

Fig. 4. Circumferential and radial stresses at the hole edge in the middle of -45° and 45° plies.

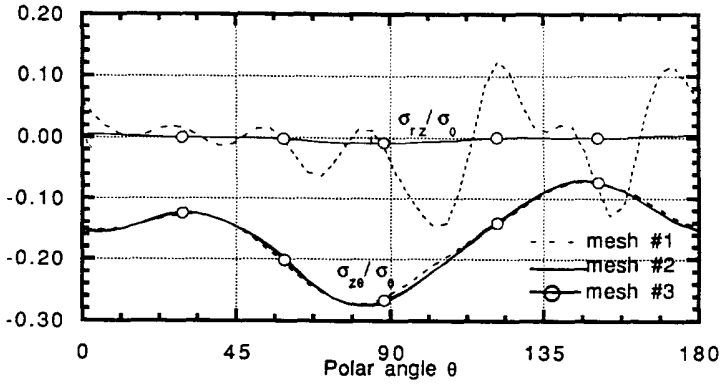

Fig. 5. Transverse shear stresses at the hole edge in the middle of the 45° ply.

subdivisions 2 and 3 were close for all meshes. The values of σ_{zz} obtained with subdivision 2 and meshes 1, 2 and 3 are shown in Fig. 6b. The study of convergence described above shows that the stress components at the hole edge of the interface between plies converge to finite limits with increasing the density of the out of plane and in plane subdivision. The stress boundary conditions at the hole edge imposed as natural boundary conditions are satisfied with higher accuracy by refining the mesh.

Comparative study included comparison of the results of circumferential stress calculation in $[90/0]_s$ laminate, considered by Chen and Huang (1989); Nishioka and Atluri (1982); and Tang (1977). The material properties were as follows: $E_1 = 207$ GPa, $E_2 = E_3 = 20.7$ GPa, $G_{13} = G_{23} = G_{12} = 10$ GPa, and $\nu_{13} = \nu_{23} = \nu_{12} = 0.336$. The radius of the hole is $R = 25$ mm and the layer thickness is $h = 5$ mm. The hole was placed in the center of a rectangular plate: $L = 0.5$ m, $A = 0.25$ m. Stresses were calculated in the middle of the 0° and 90° plies by using mesh #2 and subdivision #2. The circumferential stress

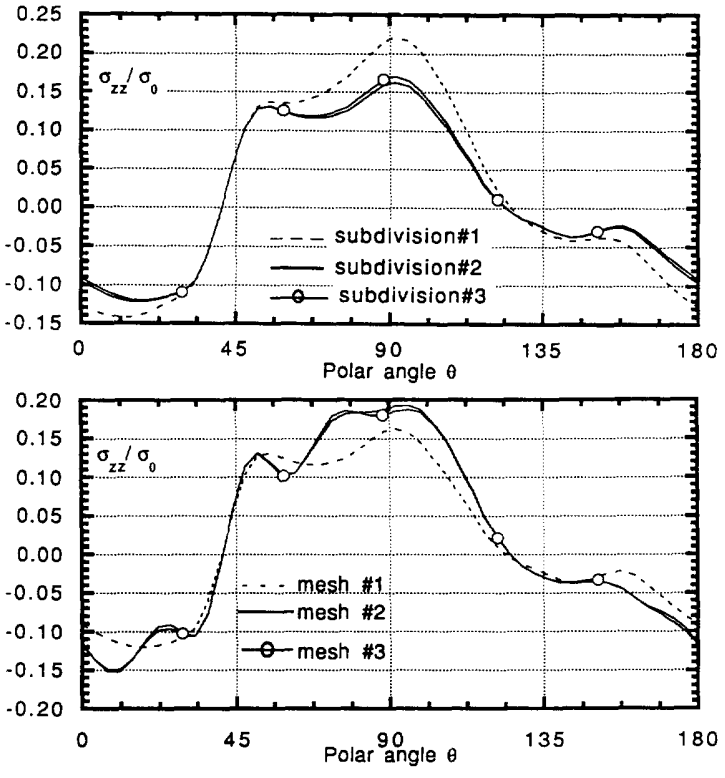

Fig. 6. σ_{zz}/σ_0 calculated at the hole edge on the mid-surface of the laminate by using different out-of-plane subdivisions—(a), and different in-plane meshes—(b).

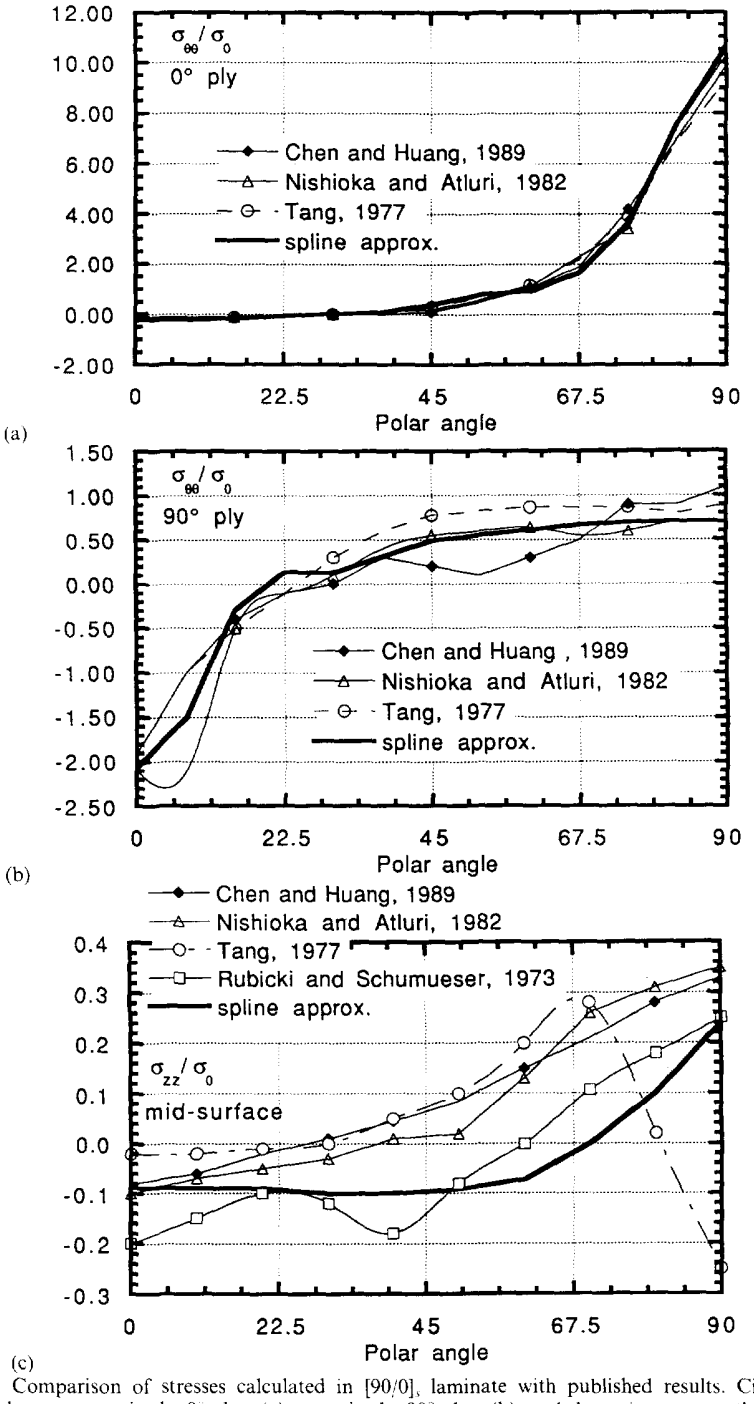

Fig. 7. Comparison of stresses calculated in [90/0]$_s$ laminate with published results. Circumferential stress $\sigma_{\theta\theta}/\sigma_0$ in the 0° ply—(a), same in the 90° ply—(b), and the σ_{zz}/σ_0 stress at the mid-surface—(c).

component $\sigma_{\theta\theta}$ in 0° ply, shown in Fig. 7a, appears to be the only characteristic upon which all considered predictions are in satisfactory agreement. The same stress component in the 90° ply is shown in Fig. 7b. In this case the differences between results obtained by different authors are significantly larger. The transverse normal stress component σ_{zz} calculated at the mid surface is displayed in Fig. 7c. For this stress component even the trends predicted by different authors are different. Neither of the results, perhaps except for the circumferential stress distribution in 0° ply, can be used for verification purposes. Due to absence of a reliable solution in the literature, an asymptotic solution of elasticity equations

is developed below and used to verify the accuracy of interlaminar stress calculation by spline approximation approach.

INTERLAMINAR STRESS CALCULATION

Stress calculation at the interlaminar surfaces in the vicinity of the hole edge is an immensely more difficult problem due to stress singularities arising at these surfaces at the hole edge, according to the theory of elasticity. A special subdivision through the thickness was introduced with the sublayer size increasing in geometric series from the interface. The interval ratio was $q = 1.5$ and the number of sublayers in each ply was equal to 6. This subdivision will be referred to as subdivision #4. To study the accuracy of interlaminar stress prediction a detailed investigation of the following stress components σ_{rz}, σ_{zz}, $\sigma_{\theta z}$, as functions of distance from the hole edge, was performed at the $-45°/45°$ interface in the $\theta = 90°$ direction. Dimensionless thickness parameter $z^* = (z - z^{(1)})/H$ has been introduced. The stress values in Figs 8a–8c shown for $z^* = -0$ are calculated in the lower ($-45°$) ply

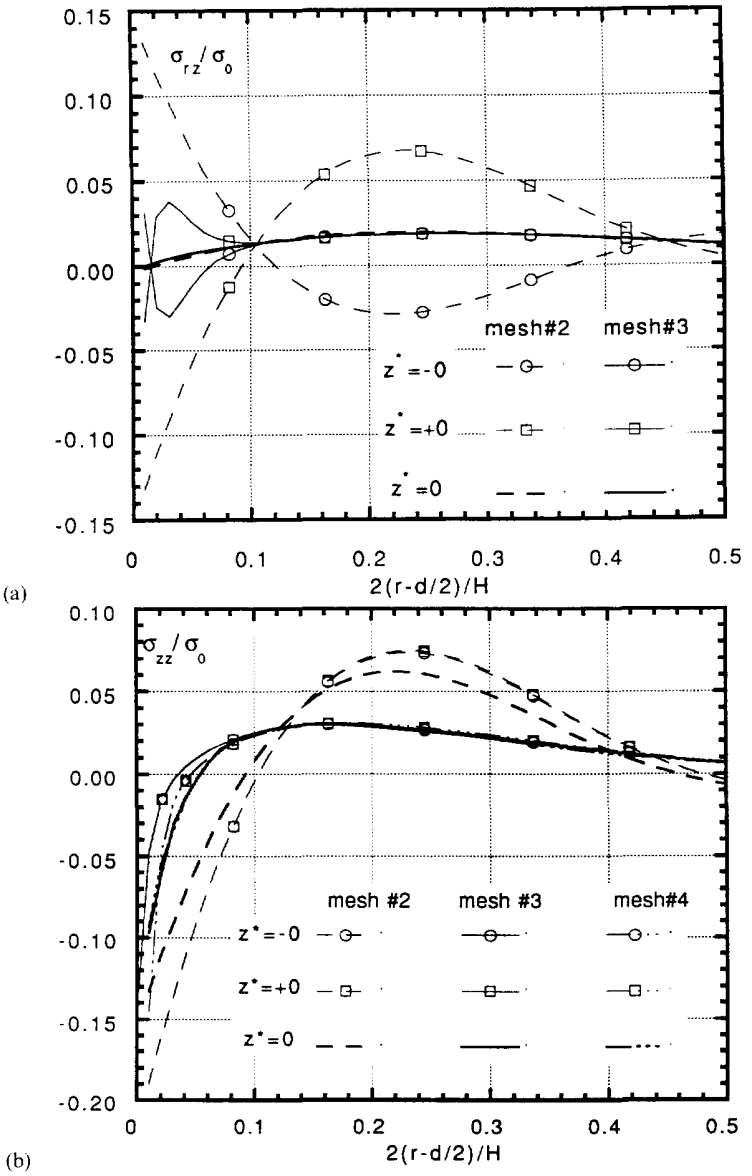

Fig. 8. Interlaminar stresses as functions of distance from the hole edge; σ_{rz}/σ_0—(a), σ_{zz}/σ_0—(b), and $\sigma_{\theta z}/\sigma_0$—(c). (*Continued overleaf.*)

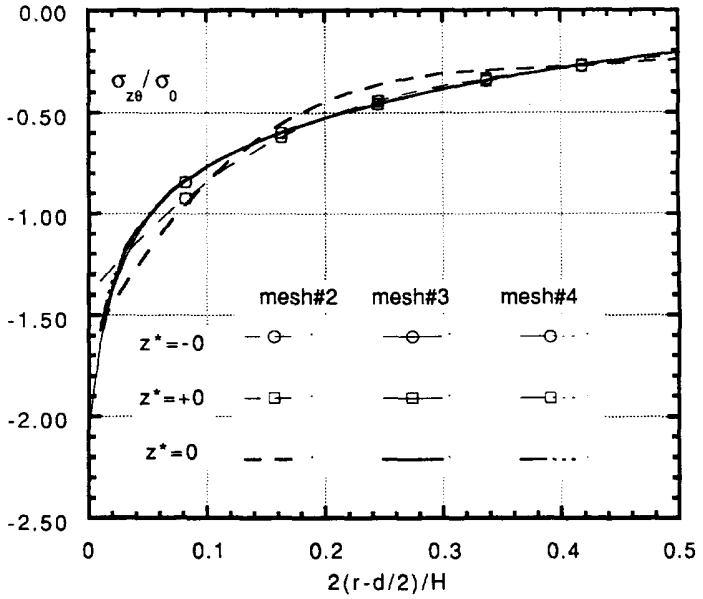

(c)

Fig. 8—(*Continued.*)

at the interface $z = z^{(1)}$ by using Hooke's law. The stress values for $z^* = +0$ are calculated at this interface also by using Hooke's law in the upper ($+45°$) ply. The stress values given for $z^* = 0$ are calculated as tractions using ply eqns (15). The stress values for $z^* = +0$, $z^* = -0$ and $z^* = 0$ have to be equal for the exact stress field starting from an infinitesimal distance from the hole edge. However, due to approximation error the accuracy of satisfying the traction continuity at the interface is mesh dependent. The σ_{rz} component calculated by using different meshes is shown in Fig. 8a. The subdivision #4 was used in all further calculations. The dense mesh #3 provides the continuity of the interlaminar stress component σ_{rz} starting from approximately $0.05H$ from the hole edge. Mesh #2 gives significant discontinuity through the distance of up to half plate thickness. The values of stresses obtained as tractions are practically equal for the two meshes. The traction value also appears to be the limit of mesh refinement for stress values obtained using Hooke's law.

The stress component σ_{zz}/σ_0 is shown in Fig. 8b. The difference between the interlaminar stress values calculated in $-45°$ ($z^* = -0$) and $+45°$ ply ($z^* = +0$) is practically zero for all meshes. However, mesh refinement shows that stress values significantly change. The criterion indicating insufficient mesh density of subdivision #2 is the difference between the traction value and the stress values obtained by using Hooke's law. A significant difference of these values obtained by using mesh #2 is observed up to $0.5H$ from the hole edge. An additional fine mesh #4 ($m = 28$, $m_0 = 24$, $q = 1.8$, smallest interval size $0.28473 \times 10^{-7}d$) was considered because the difference in stress values obtained by using meshes 2 and 3 was significant. The σ_{zz} values calculated as tractions ($z^* = 0$) for meshes 3 and 4 are practically equal. The stress values calculated by Hooke's law at distances less than $0.1H$ from the hole edge by using mesh #3 are noticeably higher than the traction values. By using finer mesh #4 they become closer to the traction values. This indicates convergence of the results by mesh refinement. Tendency similar to that for σ_{rz} is observed. The stress values calculated by Hooke's law are converging to the traction values with mesh refinement. Also, the traction values converge sooner so that they are equal for mesh #3 and 4, whereas the Hooke's law values for the two meshes differ near the hole edge.

The transverse shear $\sigma_{\theta z}/\sigma_0$ stress is considered in Fig. 8c. For coarser mesh #2 the traction value is different from the values calculated by using Hooke's law which indicates insufficient mesh density. Mesh #3 gives the traction values practically equal to stresses obtained using Hooke's law. It indicates sufficient mesh refinement, which is confirmed by the results obtained using mesh #4.

A criterion for selection of subdivision and meshing for interlaminar stress calculation is based on the maximum difference between the traction values calculated through eqns (15) and the interlaminar stress values calculated using Hooke's law. It is worth mentioning that the difference between the interlaminar stress values in two adjacent plies obtained using Hooke's law can not be used as a measure of accuracy near singular points, since it has been shown to be deceptively small even for coarse meshes.

ASYMPTOTIC ANALYSIS AND INTERLAMINAR STRESS RESULTS VERIFICATION

For asymptotic analysis a local transformation is introduced with the center $\{r = d/2, z = z^{(s)}, \theta = \theta\}$ situated at the hole edge at the interface between s and $s+1$ plies as follows:

$$r - \frac{d}{2} = \frac{d}{2}\eta\cos\psi, \quad z - z^{(s)} = \frac{d}{2}\eta\sin\psi, \quad \theta = \theta, -\pi/2 \leqslant \psi \leqslant \pi/2, \eta \geqslant 0, \quad 0 \leqslant \theta \leqslant 2\pi, \tag{16}$$

where η is a dimensionless parameter defining the distance from the hole edge, and ψ an angle defining the direction in which the singular point (center of η, ψ, θ coordinates) is approached. For an arbitrary function $F(\eta, \psi, \theta)$, one can write

$$\frac{\partial F}{\partial x} = \frac{2}{d}\left\{\Lambda_t F\cos\theta - \frac{\sin\theta}{1+\eta\cos\psi}\frac{\partial F}{\partial\theta}\right\}, \frac{\partial F}{\partial y} = \frac{2}{d}\left\{\Lambda_t F\sin\theta + \frac{\cos\theta}{1+\eta\cos\psi}\frac{\partial F}{\partial\theta}\right\} \quad \frac{\partial F}{\partial z} = \frac{2}{d}\Lambda_n F \tag{17}$$

where

$$\Lambda_t F = \cos\psi\frac{\partial F}{\partial\eta} - \frac{\sin\psi}{\eta}\frac{\partial F}{\partial\psi}, \quad \Lambda_n F = \sin\psi\frac{\partial F}{\partial\eta} + \frac{\cos\psi}{\eta}\frac{\partial F}{\partial\psi}.$$

For $\eta \ll 1$ the terms containing $\partial F/\partial\theta$ vanish in eqns (17). It means that the stresses obtained from the asymptotic analysis are defined with accuracy of an arbitrary additive—a function of the θ coordinate. The equations of equilibrium for the s-th ply can be written as

$$\{\mathbf{A}\Lambda_t\Lambda_t + \mathbf{B}\Lambda_t\Lambda_n + \mathbf{C}\Lambda_n\Lambda_n\}\begin{pmatrix} u_x \\ u_y \\ u_z \end{pmatrix} = 0 \tag{18}$$

where the symmetric square (3×3) matrices **A**, **B**, **C** have the following coefficients:

$$A_{11} = Q_{11}^{(s)}\cos^2\theta + Q_{16}^{(s)}\sin 2\theta + Q_{66}^{(s)}\sin^2\theta,$$

$$A_{12} = Q_{16}^{(s)}\cos^2\theta + (Q_{12}^{(s)} + Q_{66}^{(s)})\sin\theta\cos\theta + Q_{62}^{(s)}\sin^2\theta,$$

$$A_{22} = Q_{61}^{(s)}\cos^2\theta + Q_{26}^{(s)}\sin 2\theta + Q_{22}^{(s)}\sin^2\theta, \quad A_{33} = Q_{55}^{(s)}\cos^2\theta + Q_{54}^{(s)}\sin 2\theta + Q_{44}^{(s)}\sin^2\theta,$$

$$A_{21} = A_{12}, \quad A_{31} = A_{13} = A_{32} = A_{23} = 0,$$

$$B_{31} = (Q_{13}^{(s)} + Q_{55}^{(s)})\cos\theta + (Q_{63}^{(s)} + Q_{54}^{(s)})\sin\theta, \quad B_{32} = (Q_{63}^{(s)} + Q_{45}^{(s)})\cos\theta + (Q_{23}^{(s)} + Q_{44}^{(s)})\sin\theta,$$

$$B_{21} = B_{12} = B_{11} = B_{22} = B_{33} = 0, \quad B_{13} = B_{31}, \quad B_{23} = B_{32},$$

$$C_{11} = Q_{55}^{(s)}, \quad C_{12} = Q_{54}^{(s)}, \quad C_{22} = Q_{44}^{(s)}, \quad C_{33} = Q_{33}^{(s)},$$

$$C_{21} = C_{12}, \quad C_{31} = C_{11} = C_{32} = C_{23} = 0.$$

Contracted notation for stiffness and stress components will be used if not identified otherwise. Indices $i,j = 1,\ldots,6$ correspond to xx, yy, zz, zy, zx, xy respectively. It can be shown that eqn (18) is consistent with those derived by Wang and Lu (1993) under the assumption that the ply thickness is small compared to the hole diameter. In the present solution this assumption is replaced with the weaker assumption $\eta \ll 1$ implying that the quasi-two dimensional eqn (18) is valid in the vicinity of the hole edge near the interface of two plies with arbitrary thickness. A straight forward solution technique for eqn (18) is based on the fact that any function of the argument $\omega = \eta(\sin\psi + \mu\cos\psi)$, is a generalized eigenfunction for the pair of commutative operators Λ_t and Λ_n so that

$$\Lambda_t F(\omega) = \mu\Lambda_n F(\omega) \tag{19}$$

where μ is an arbitrary complex constant. Restricting the eigenfunctions to the class $F(\omega) = F_1(\eta)F_2(\psi)$ we find that the only solutions of (19) left are of the form $F(\omega) = \omega^\lambda$, λ is an arbitrary complex number. The general solution for eqn (18) can be found as a superposition of solutions $(u_x, u_y, u_z)^* = \omega^\lambda \mathbf{d}$, where $\mathbf{d}$ is an unknown constant complex vector. Substituting this expression into eqn (15) we arrive at a sixth order polynomial characteristic equation

$$\det|\mathbf{A}\mu^2 + \mathbf{B}\mu + \mathbf{C}| = 0. \tag{20}$$

For a ply with orthotropic material properties and θ different from any of the directions of it's principle material axes, eqn (20) has six different roots, such that $\mu_k = -\mu_{k+3}$, $k = 1, 2, 3$. The general solution of eqn (18) can be expressed as

$$(u_x, u_y, u_z)^* = \sum_{k=1}^{6} f_k \mathbf{d}_k \eta^\lambda (\sin\psi + \mu_k \cos\psi)^\lambda \tag{21}$$

where f_k and λ are arbitrary complex constants to be defined from the boundary conditions. In case of the orthotropic ply and θ coinciding with one of its principle material axes, eqn (20) will have two roots of multiplicity 2. For an isotropic ply one will find that $\mu_1 = \mu_2 = \mu_3 = i$ and $\mu_4 = \mu_5 = \mu_6 = -i$, where $i = \sqrt{-1}$. In these cases solution (21) has to be modified. The intended application of this asymptotic solution is beyond the two particular cases mentioned above and can be described by the general solution (21). The expressions for calculating the stress components in xyz coordinates in each ply for $\eta \ll 1$ are as follows:

$$\begin{aligned}
\sigma_i = {} & \frac{2\lambda\eta^{\lambda-1}}{d} \sum_{k=1}^{6} f_k (\sin\psi + \mu_k\cos\psi)^{\lambda-1} [\mu_k((Q_{i1}\cos\theta + Q_{i6}\sin\theta)\{\mathbf{d}_k\}_1 \\
& + (Q_{i1}\cos\theta + Q_{i2}\sin\theta)\{\mathbf{d}_k\}_2) + Q_{i3}\{\mathbf{d}_k\}_3], \quad i = 1,2,3,6, \\
\sigma_i = {} & \frac{2\lambda\eta^{\lambda-1}}{d} \sum_{k=1}^{6} f_k (\sin\psi + \mu_k\cos\psi)^{\lambda-1} [Q_{i5}\{\mathbf{d}_k\}_1 + Q_{i4}\{\mathbf{d}_k\}_2 \\
& + \mu_k(Q_{i5}\cos\theta + Q_{i4}\sin\theta)\{\mathbf{d}_k\}_3], \quad i = 4,5,
\end{aligned} \tag{22}$$

where stress components σ_i correspond to σ_{xx}, σ_{yy}, σ_{zz}, σ_{yz}, σ_{zx}, σ_{xy} for $i = 1,\ldots,6$ correspondingly. The ply number is not shown since only the elastic moduli of one ply enter eqn (22). The unknown coefficients f_k have to be obtained from the boundary conditions on the interface between s and $s+1$ plies and the free edge of the hole. The boundary conditions at the interface between s and $s+1$ plies are as follows:

$$\begin{gathered}
u_x^{(s)} = u_x^{(s+1)}, \quad u_y^{(s)} = u_y^{(s+1)}, \quad u_z^{(s)} = u_z^{(s+1)}, \\
\sigma_{zz}^{(s)} = \sigma_{zz}^{(s+1)}, \quad \sigma_{zx}^{(s)} = \sigma_{zx}^{(s+1)}, \quad \sigma_{zy}^{(s)} = \sigma_{zy}^{(s+1)} \quad \text{at } \psi = 0.
\end{gathered} \tag{23}$$

Six conditions (20) are used to determine a complex 6×6 matrix which establishes a unique relationship between the coefficients $\mathbf{f}^{(s)} = \{f_k^{(s)}\}_{k=1}^{6}$ for the s-th ply and those for the $s+1$. The boundary conditions at the free edge of the hole in the s-th ply are written as

$$\sigma_{rr}^{(s)} = \sigma_{zr}^{(s)} = \sigma_{\theta r}^{(s)} = 0, \quad \psi = -\frac{\pi}{2}.$$

These three equations are expressed through the coefficients for the $s+1$ ply using the matrix established before. Combined with the following free edge boundary conditions for the $s+1$ ply:

$$\sigma_{rr}^{(s+1)} = \sigma_{zr}^{(s+1)} = \sigma_{\theta r}^{(s+1)} = 0, \quad \psi = +\frac{\pi}{2}$$

they form a homogeneous system of six linear equations with unknowns $f_k^{(s+1)}$, $k = 1, \ldots, 6$. To assure an existence of a non trivial solution the parameter λ is obtained by requiring the determinant of this system to be equal to zero. The transcendental equation for λ has an infinite number of roots. Only the roots $0 < \mathrm{Re}\,(\lambda_j) < 1$ were obtained. The determinant of a 6×6 matrix was calculated directly using permutation algorithm. The initial approximation for the first root was defined by calculating the determinant for real values of $\lambda = 0.99, 0.98, 0.97, \ldots$ until a change of sign of the real part of the determinant was detected. The roots were refined using Mueller's method. The two λ values between which the sign has changed and the half sum of these two values were utilized as three initial values for Mueller's method. After the root λ_1 was obtained the process was repeated for $\lambda_2 = \lambda_1 - 0.01, \ldots$ until all roots with $0 < \mathrm{Re}\,(\lambda_j) < 1$ were obtained. It is essential to point out that the value $\lambda = 1$ will also be a root as well as all integers. For a given root value of λ the coefficients $f_k^{(s-1)}, k = 1, \ldots, 6$ and $f_k^{(s)}, k = 1, \ldots, 6$ can only be obtained to within an arbitrary multiplicative factor. It was always assumed that $f_1^{(s)} = 1$. The stress components satisfying eqns (18) can be represented as

$$\sigma_i = F_i(\theta) + \sum_{j=1}^{\infty} f_j \eta^{\lambda_j - 1} \bar{\sigma}_j(\lambda_j, \psi, \theta), \quad i = 1, \ldots, 6 \tag{24}$$

where expressions for quantities with bars can be established by comparing with eqns (22). The additives $F_i(\theta)$, independent of local coordinates, are introduced since the eqns (18) define the solution within accuracy of a function of θ. Coefficients f_j and functions $F_i(\theta)$ can only be obtained from the full field solution. It is worth while to emphasize that series (24) will not provide the full field solution to the three-dimensional problem no matter how many expansion terms are used, because for $\eta \approx 1$ the terms containing $\partial F/\partial\theta$ will not vanish in expressions (17) and thus the eqns (18) will be invalid. For small $\eta \ll 1$, however, the full field solution is expected to correlate with the singular term of the expansion (24).

The $[45/-45]_S$ laminate used for convergence study will be considered. The asymptotic analysis performed at the $45/-45$ interface revealed only one root such that $0 < \mathrm{Re}(\lambda_1) < 1$ for every θ value. It was also checked that this root has a zero imaginary part. The distribution of λ_1 vs θ is shown in Fig. 9. To match the asymptotic and full field numerical solutions the values of coefficients f_j in eqns (21) are needed. Let us consider the stress components as functions of distance from the hole edge at $\theta = 90^\circ$. The distribution of $\sigma_{\theta r}$ stress obtained by using full field spline approximation and the asymptotic solution are shown in Fig. 10. Only the first term of the asymptotic solution in series (24) corresponding to the $\lambda_1 = 0.961$ is accounted for. The value of the arbitrary multiplicative factor for the first term of series (24) was chosen equal to $f_1 = -2.231\sigma_0$. The stresses are shown in 45 and -45 plies at the interface and at two plains parallel to the interface. Parameter z^* was equal to ± 0.06 and ± 0.024 defining surfaces close to the interface in 45 ply for positive z^* and in the -45 ply for negative z^*. On this and the following figures solid lines will be used to display the results of spline approximation solution and dashed lines the results of

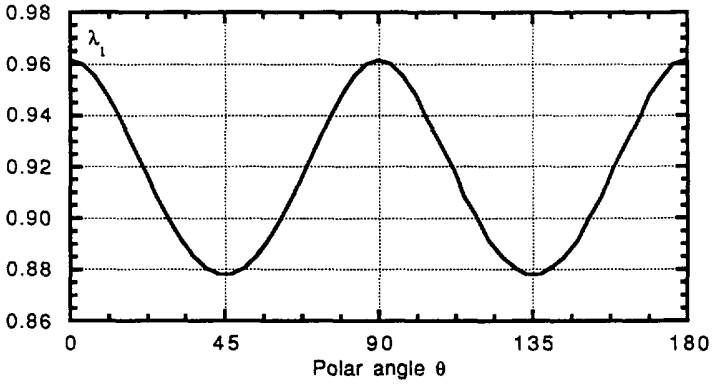

Fig. 9. The power of singularity as a function of polar angle.

asymptotic analysis. Excellent agreement between the full field spline solution and one term asymptotic solution for distances up to $H/4$ from the hole edge is observed. Such a good agreement between full field and asymptotic solution can be explained because the values of $\sigma_{r\theta}$ at $\theta = 90^\circ$ are different from zero only due to higher order effects, such as interlaminar tractions. Indeed, in lamination theory solution this stress is equal to zero due to symmetry. Thereby, the effect of the terms corresponding to $\lambda_2, \ldots$ in series (24) is very small. At the interface on distances less than $0.01H$ from the hole edge the asymptotic solution shows a rapid increase of amplitude, whereas the amplitude of the numerical solution changes in other direction. The explanation, proposed by Pagano (1995), takes into account the non uniqueness of stress amplitude at $\eta = 0$ predicted by the asymptotic solution depending upon the direction in which the singular point is approached. Figure 11 shows the amplitudes of the singular stresses predicted by the asymptotic solution as functions of direction ψ. The polar angle is $\theta = 90^\circ$. Only two stress components σ_{zz} and $\sigma_{\theta z}$ have a practically constant amplitude of singular stress near $\eta = 0$ for all ψ. Only for these stresses can a meaningful comparison between the asymptotic and numerical solution be expected at very small η values. Figures 12a and 12b show the σ_{zz} and $\sigma_{\theta z}$ stresses correspondingly. The coefficient $f_1 = -2.231$ obtained for the $\sigma_{\theta r}$ stress component was used with the singular term. A constant was added to the single term approximation in (24) to account for the contribution of higher order terms. The functions plotted in Figs 12a and 12b as asymptotic solutions are as follows

$$\sigma_{zz}/\sigma_0 = -2.231\eta^{\lambda_1 - 1}\bar{\sigma}_{zz}(\lambda_1, \psi) + 3.371, \quad \sigma_{\theta z}/\sigma_0 = -2.231\eta^{\lambda_1 - 1}\bar{\sigma}_{\theta z}(\lambda_1, \psi) + 9.192.$$

The constants were obtained by requiring the asymptotic and numerical solutions to comply at one point $z^* = 0.024$, $r\text{-}d/2 = 0.032H/2$. These constants account for unknown functions $F_i(\theta)$ and the contribution of the second term $\lambda_2 = 1.0$ in series (21). This term according

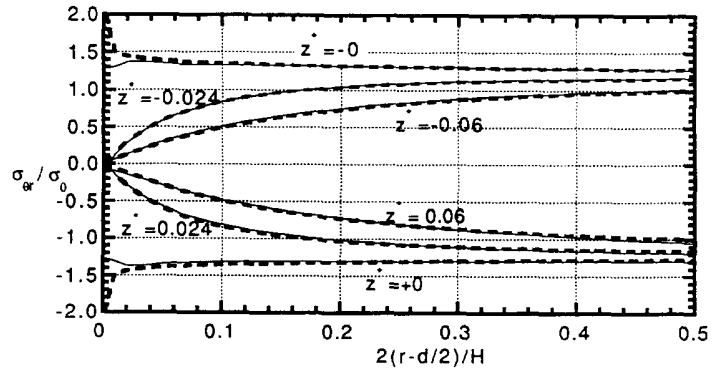

Fig. 10. The distribution of $\sigma_{\theta r}/\sigma_0$ stress vs distance from the hole edge at the interface and at parallel surfaces.

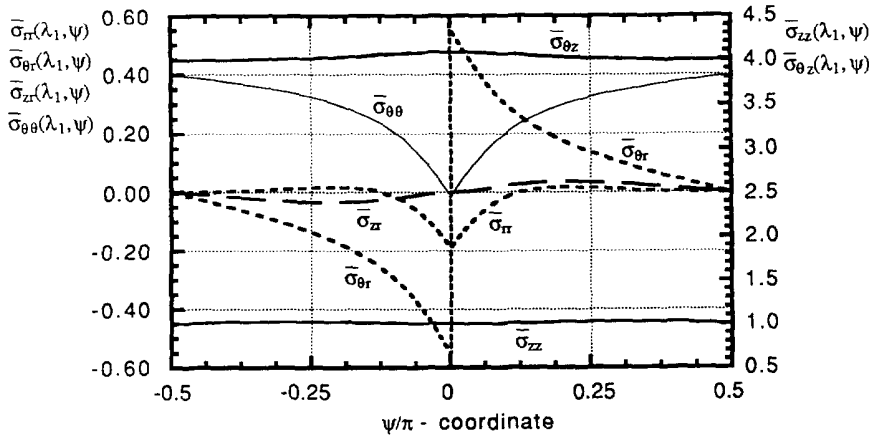

Fig. 11. Amplitudes of the singular stresses predicted by the asymptotic solution as a functions of local coordinate ψ for $\theta = 90°$.

to (22) yields stress values independent of the local variables η and ψ and thus is determined by full field solution. It is worth mentioning that the asymptotic and spline approximation methods describe a sharp minimum of σ_{zz} stress for $z^* = -0.024$ which can be observed at a distance $r = 0.0005H$ from the hole edge in Fig. 12a. The distribution of the $\sigma_{\theta z}$ stress, shown in Fig. 12b, is rather smooth and also persuades an excellent agreement between the spline approximation and asymptotic solutions. In Figs 13a–13c the stress components $\sigma_{\theta\theta}$, σ_{rz} and σ_{rr}, obtained by spline approximation solution, are compared to the asymptotic solutions calculated for each stress component as follows:

$$\sigma_{\theta\theta}/\sigma_0 = -2.231\rho^{\lambda_1-1}\bar{\sigma}_{\theta\theta}(\lambda_1,\psi)+2.753, \quad \sigma_{rz}/\sigma_0 = -2.231\rho^{\lambda_1-1}\bar{\sigma}_{rz}(\lambda_1,\psi),$$

$$\sigma_{rr}/\sigma_0 = -2.231\rho^{\lambda_1-1}\bar{\sigma}_{rr}(\lambda_1,\psi).$$

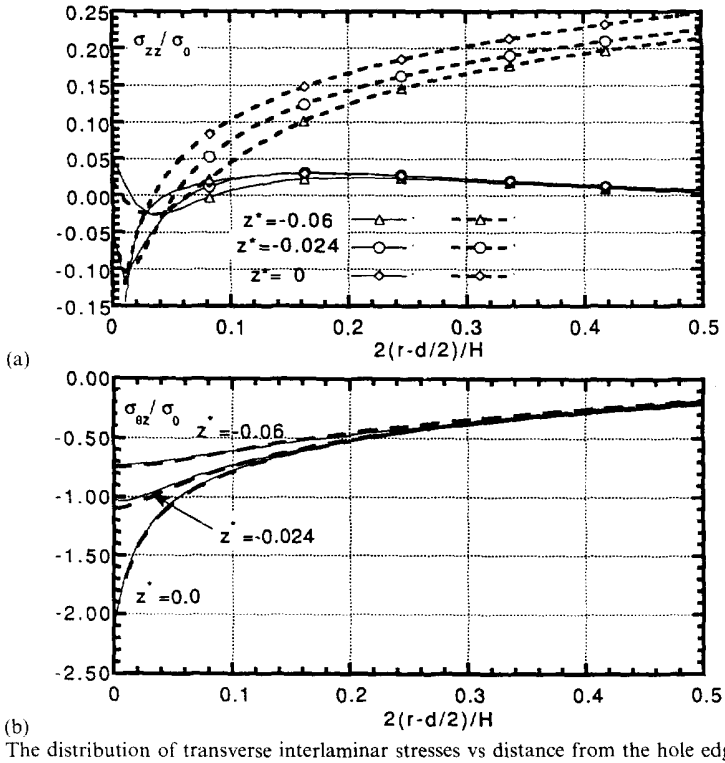

Fig. 12. The distribution of transverse interlaminar stresses vs distance from the hole edge at the interface and at parallel surfaces; σ_{zz}/σ_0—(a), $\sigma_{\theta z}/\sigma_0$—(b).

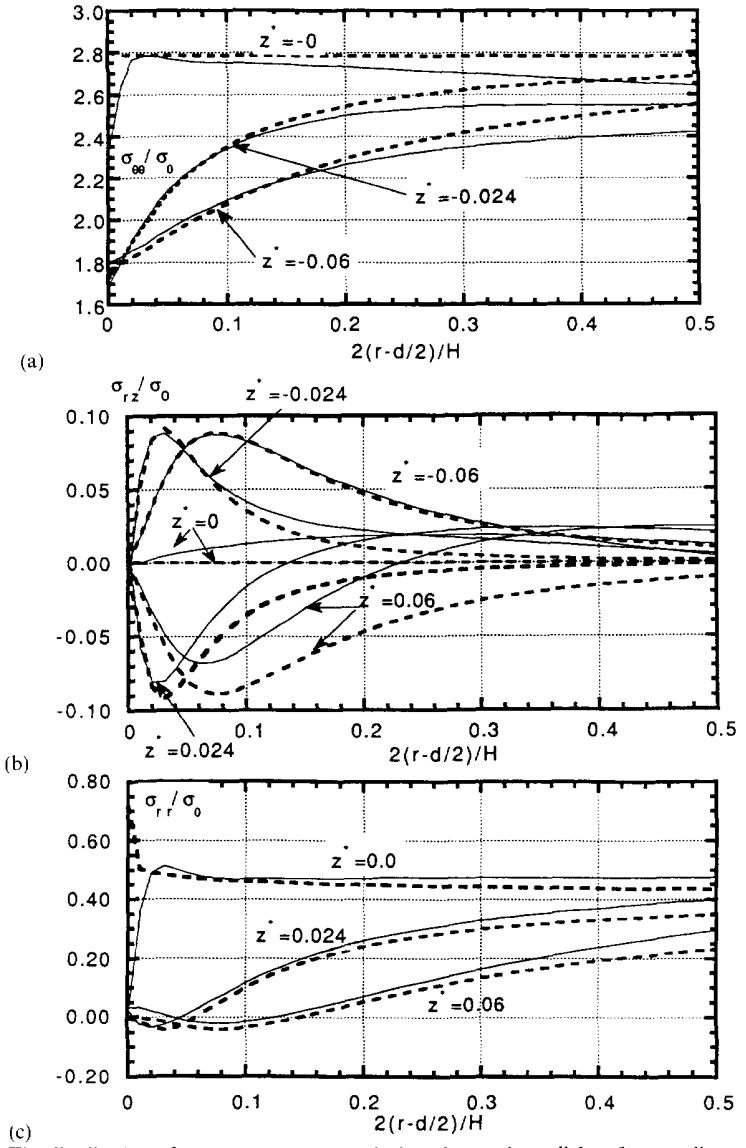

Fig. 13. The distribution of stress components at the interface and parallel surfaces vs distance from the hole edge: $\sigma_{\theta\theta}/\sigma_0$—(a), σ_{rz}/σ_0—(b), σ_{rr}/σ_0—(c).

The constant, related to second term $\lambda_2 = 1.0$ in series (21), for the $\sigma_{\theta\theta}$ component was calculated as described above for $\sigma_{\theta z}$ and σ_{zz}. For stress components σ_{rz} and σ_{rr} entering the boundary conditions (24) this term must be apparently equal to zero. The circumferential stress component in Fig. 13a and the σ_{rz} stress in Fig. 13b are influenced by higher order terms of series (24). However, good agreement for stresses in the vicinity of the interface is observed. The radial stress component is shown in Fig. 13c. At the interface for the distances less than $0.01H$ from the hole edge the spline approximation solution tries to satisfy the natural boundary condition of zero radial stresses. The exact asymptotic solution on the other hand satisfies these conditions only for $\psi = \pm\pi/2$. By approaching the hole edge along the interface, i.e. $\psi = 0$ the radial stress grows infinitely as shown in Fig. 13c. Overall the agreement between the spline approximation and asymptotic solution results is obvious.

CONCLUSIONS

A numerical procedure based on independent polynomial spline approximation of the displacement and interlaminar stress components in curvilinear coordinates is proposed for

solving boundary value problems in laminated composites. The procedure is ideally suited for problem treatments containing regions of solution singularity. A full field solution for composite plates containing open hole is obtained. Converged stresses and consistent boundary conditions, such as interlaminar traction continuity, are displayed.

An asymptotic elasticity solution has been derived for stress distributions near open hole edge at the interface between two orthotropic plies of arbitrary thickness. Good agreement between the spline approximation full field solution results and the asymptotic solution were observed in the vicinity of the hole edge for all stress components.

Acknowledgment—The work was funded by the Materials Directorate, Wright Laboratory, WL/MLBM, Wright-Patterson AFB OH under Contract No. F33615-88-C-5420. The author expresses his sincere appreciation to Dr R. Hall and Capt. D. Rose of WL/MLBM, and Dr S. R. Soni and Dr J. Ahmad of AdTech System Research, Inc. for support and fruitful discussions at all stages of the work.

The author is deeply indebted to Dr N. J. Pagano who reviewed the entire manuscript and offered numerous valuable suggestions.

REFERENCES

Bar-Yoseph, P. and Avrashi, G. (1985). Interlaminar stress analysis for laminated plates containing a curvilinear hole. *Computers Struct.* **21,** 917–932.

Bogdanovich, A. E. and Iarve, E. V. (1992). Numerical analysis of impact deformation and failure in composite plates. *J. Comp. Mat.* **26,** 520–545.

Bogdanovich, A. E., Iarve, E. V. and Joshi, S. P. (1990). Impact deformatio.. and failure analysis of laminated composite plates. *Impact and Buckling of Structures, Proceedings of the Winter Annual Meeting of the ASME*, pp. 1–5 AD-Vol. 20, Dallas. ASME, New York.

Bogdanovich, A. E. and Iarve, E. V. (1989a). Numerical analysis of composite plates subjected to impact loading. In *Proc. ASC Fourth Technical Conference*, pp. 399–409, Blacksburg, October (1989).

Bogdanovich, A. E. and Yarve, E. V. (1989b). Numerical analysis of the impact deformation of plates made of composites. *Mech. Comp. Mat.* **25,** 586–599 (translated from Russian by Consultants Bureau, New York, March, 1990).

Bogdanovich, A. E. and Yarve, E. V. (1988). Numerical solution of two-dimensional problem of non-steady deformation of laminated media. *Mech. Comp. Mat.* **24,** 31–38 (translated from Russian by Consultants Bureau, New York, July, 1988).

Bogdanovich, A. E. and Yarve, E. V. (1983). Stress analysis in multilayered beams under transverse dynamic bending. *Mech. Comp. Mat.* **19,** 604–616 (translated from Russian by Consultants Bureau, New York, March, 1984).

Bogdanovich A. E. and Birger A. B., (1994). Three-dimensional stress field analysis in uniformly loaded, simply supported composite plates. *Computers Struct.* **52,** 237–257.

Bogdanovich A. E., (1992). Spline function aided analysis of inhomogeneous materials and structures. In *Proc. IUTAM Symposium Local Mechanics Concepts for Composite Material Systems*, pp. 355–382, Blacksburg, VA 1991, Springer-Verlag, Berlin, New York.

Bogdanovich, A. E. and Birger, A. B., (1992). Application of spline functions to the 3-D analysis of laminated composite plates subject to static bending. In *Proc. 2nd International Symposium on Composite Materials and Structures*, pp. 719–725, 3–7 August 1992, Beijing. Beijing University Press, Beijing, China.

Bogdanovich, A. E. and Birger, A. B., (1992). Application of spline functions to the analysis of local boundary effects in laminated composite plates. In *Proc. ASME Winter Annual Meeting, Symposium on Damage Mechanics in Composites*. AMD Vol. 150/AD Vol. 32, pp. 275–293, Anaheim, CA, 1992. The ASME Publication.

Bogdanovich, A. E. and Birger, A. B., (1993). Stress fields and initial failure in a cantilever laminated composite plate under transverse and in-plane loads. In *Proc. 1st Joint Mechanics Meeting of ASME/ASCE/SES, Non-Classical Problems of the Theory and Behavior of Structures Exposed to Complex Environmental Conditions*, AMD Vol. 164, pp. 155–167, Charlottesville, VA, June 6–9, 1993. The ASME Publication.

Bogdanovich, A. E. (1993). Three-dimensional analysis of laminated composite plates. In *Advanced Composites '93, International Conference on Advanced Composite Materials*, Wollongong, Australia, 15–19, February 1993, pp. 79–91, TMS Minerals/Metals/Materials, Wollongong.

Chen, W. H. and Muang, T. F. (1989). Three-dimensional interlaminar stress analysis at free-edges of composite laminate. *Computers Struct.* **32,** 1275–1286.

Ericson, K., Persson, M., Carlsson, L. and Gustavsson, A. (1984). On the prediction of the initiation of delamination in a $[0/90]_s$ laminate with a circular hole. *J. Comp. Mat.* **8,** 495–506.

Folias, E. S. (1989). On the interlaminar stresses of a composite plate around the neighborhood of a hole. *Int. J. Solids Struct.* **25,** 1193–1200.

Folias, E. S. (1992). Boundary layer effects of interlaminar stresses adjacent to a hole in a laminated composite plate. *Int. J. Solids Struct.* **29,** 171–186.

Garbo, S. P. and Ogonowski, J. M. (1979). Strength predictions of composite laminates with unloaded fastener holes. *AIAA J.* **18** 585–588.

Iarve, E. V. (1993). Interlaminar stress analysis in compression loaded composite plates containing open hole. In *Proc. ASC Eighth Technical Conference*, pp. 1025–1034, Clevland OH, 19–21 October.

Iarve, E. V. and Soni S. R. (1993). Stress analysis in compression loaded rectangular composite plates containing open hole. In *ICCM-9 Proceedings* **III,** pp. 135–142, Madrid, 12–16 July.

Iarve, E. V. and Soni S. R. (1993). Three-dimensional stress analysis in compression loaded laminates containing open hole. In *Composite Materials and Structures, Proc. Winter Annual Meeting of the ASME*, AD-Vol. 37, pp. 117–132, New Orleans, November 29–December 5.

Iarve, E. V., (1994). On the accuracy of interlaminar stress calculation in the vicinity of an open hole in composite by use of spline variational technique. In *Proc. ASC Ninth Technical Conference*, pp. 1025–1034, Delaware, DE, 19–21 November.

Lekhnitskii, S. G. (1957). *Anisotropic Plates*. Gos. Isdat., Moscow.

Lucking, W. M., Hoa, S. V. and Sankar, T. S. (1984). The effect of geometry on interlaminar stress of $[0/90]_s$ composite laminates with circular holes. *J. Comp. Mat.* **17,** 188–198.

Nishioka, T. and Atluri, S. N. (1982). Stress analysis of holes in angle-ply laminates: an efficient assumed stress special-hole-element approach and a simple estimation method. *Computers Struct.* **15,** 135–147.

Pagano, N. J. (1971). On the calculation of interlaminar normal stress in composite laminates. *J. Comp. Mat.* **5,** 50.

Pagano, N. J. (1978). Free edge stress field in composite laminates. *Int. J. Solids Struct.* **14,** 401–406.

Pagano, N. J. and Kaw, A. K. (1995). Asymptotic stresses around the crack tip at the interface between planar or circular bodies. *Int. J. Fract.* (to appear).

Raju, I. S. and Crews, J. H., Jr. (1982). Three-dimensional analysis of $[0/90]_s$ and $[90/0]_s$ laminates with a central circular hole. *Comp. Tech. Rev.* **4,** 116–124.

Tang, S. (1979). A variational approach to edge stresses of circular cutouts in composites. *AIAA/ASME/ASCE/AHS, S.M.D. Conference*, pp. 326–332, St Louis, MO.

Tong, P. and Pian, T. H. H (1973). On the convergence of the finite element method for problems with singularity. *Int. J. Solids Struct.* **9,** 313–321.

Wang, S. S. and Choi, I. (1982). Boundary-layer effects in composite laminates: part 1-free-edge stress singularities. *J. Appl. Mech.* **49,** 541–560.

Wang, S. S. and Lu, X. (1993). Three-dimensional asymptotic solutions for interlaminar stresses around cutouts in fiber composite laminates. *Mech. Thick Comp.* **AMD-Vol. 162,** 41–50.